International Journal of Engineering

Journal Homepage: www.ije.ir

Heat Transfer Enhancement of a Flat Plate Boundary Layer Distributed by a Square Cylinder: Particle Image Velocimetry and Temperature-Sensitive Paint Measurements and Proper Orthogonal Decomposition Analysis

G. Ghassabi*[a], M. Kahrom[b]

[a] *Department of Mechanical Engineering, Engineering faculty, Bozorgmehr University of Qaenat, Qaen, Iran*
[b] *Department of Mechanical Engineering, Ferdowsi University of Mashhad, Mashhad, Iran*

PAPER INFO

Paper history:
Received 06 July 2018
Received in revised form 22 August 2018
Accepted 26 October 2018

Keywords:
Heat transfer coefficient
Reverse flow
Reattachment point
Eigenmode

ABSTRACT

The current empirical study was conducted to investigate the wall neighborhood impact on the two-dimensional flow structure and heat transfer enhancement behind a square cylinder. The low- velocity open-circle wind tunnel was used to carry out the study tests considering the cylinder diameter (D)-based Reynolds number (Re_D) of 5130. The selected items to compare were different gap height (G/D= 0.0, 0.1, 0.2 and 0.8). The flow field was measured using particle image velocimetry (PIV) with high image-density camera. The PIV-derived time-averaged quantities, including the streamline pattern, streamwise velocity fluctuation intensity, and reverse-flow intermittency, were examined for the flow past the square cylinder. The measurements of PIV were decomposed with the help of proper orthogonal decomposition (POD) approach that provides a proper view of the POD modes. To obtain the value of the heat transfer enhancement behind the square cylinder, the full-field temperature distributions of flat plate were measured through the temperature-sensitive paint (TSP) technique. Results showed that the maximum heat transfer enhancement was obtained at G/D=0.2 due to the high unstable flow near the wall.

***doi**: 10.5829/ije.2018.31.11b.21*

NOMENCLATURE

D	Cylinder diameter (m)	**Greek Symbols**	
G	Gap height (m)	γ_t	Reverse flow intermittency
h	Local heat transfer coefficient (W/m^2.k)	δ	The thickness of the boundary layer
h_0	Local heat transfer coefficient without cylinder (W/m^2.k)		
I	Ampere (A)		

1. INTRODUCTION

Flow behind the bluff body near the wall has found in many practical situations such as heat exchanger, suspension bridge, pipes near the ground, flow past buildings, etc. Therefore, many studies were performed about flow structure, heat transfer, drag and lift behind the simple bluff body like cylinders near the wall.

*Corresponding Author Email: *Ghodrat.ghassabi@buqaen.ac.ir* (G. Ghassabi)

Wall heat transfer behind the cylinder was investigated in recent decades. Marumo et al. [1] compared experimentally the value of the heat transfer coefficient of the flat plate with and without the circular cylinder insert near the plate. They used a hot wire method for flow measurements. They also studied the effect of gap height on heat transfer enhancement. Their results showed that there is an optimum gap height for the maximum heat transfer enhancement. This result was also given by other researchers for circular cylinder [2]. Suzuki et al. [3] studied the effect of the circular cylinder size and gap height on the heat transfer

Please cite this article as: G. Ghassabi, M. Kahrom, Heat Transfer Enhancement of a Flat Plate Boundary Layer Distributed by a Square Cylinder: Particle Image Velocimetry and Temperature-Sensitive Paint Measurements and Proper Orthogonal Decomposition Analysis, International Journal of Engineering (IJE), IJE TRANSACTIONS B: Applications Vol. 31, No. 11, (November 2018) 1962-1971

coefficient of the flat plate. The study indicated that the gap height was more effective than the cylinder size in heat transfer coefficient. Inaoka et al. [4] placed a square insert in the turbulent boundary layer and numerically evaluated the heat transfer coefficient. Their results represented that the heat transfer coefficient increased by inserting the cylinder. They also found the same result for the laminar flow [5]. Inaoka et al. [6] studied the effect of a splitter plate attached to behind the square cylinder on heat transfer enhancement. Results show that by increasing the length of the splitter plate, the effect of Karman vortex on the flat plate decreases. Therefore, increasing the length of the splitter plate lead to a decline in the value of heat transfer enhancement. This result was also given by other researchers [7, 8]. De souza et al. [9] used hot wire technique investigated heat transfer and wall skin friction in a turbulent boundary layer interacting with a cylinder wake. They found that the obvious dissimilarity of heat with momentum transfer in the disturbed boundary layer could be effectively influenced by the large-scale coherent structures. Kahrom et al. [10, 11] reported the highest heat transfer by optimizing the dimension of a quad insert and the gap height. Kahrom in another research [12] investigated the effect of this optimum insert on heat transfer of a domestic gas burner. Ghorbani et al. [13] studied the effect of the height of rectangular bluff buddies on wall heat transfer enhancement. The results showed that Heat transfer enhancement is sensitive to blockage ratio. In another study, they [14] investigated the influence of rectangular-in-tandem on wall heat transfer with different spacing-to-span-wise widths (S/d). The results showed that the maximum heat transfer was achieved for S/d=4.

Studies of flow structure behind the cylinder near the wall are mainly focused on vortex shedding, body force, and pressure measurement. There are several methods to show flow structure, such as hot-wire anemometry (HWA), hot-film anemometry (HFA), laser Doppler anemometry (LDA), PIV, etc. Bearman and Zdravkovich [15] using (HWA) investigated vortex shedding of the circular cylinder near the wall for some gap heights. They found that the vortex shedding was removed for (G/D< 0.3). Martinuzzi et al. [16] determined the influence of the gap height on lift and drag using (LDA). The study demonstrated that drag decreases by decreasing the gap height. Shi et al. [17] studied the effect of the gap height on velocity distribution using (PIV). The results showed that the vortices expand as the gap height decreased. Raiola et al. [18] explored the wake behind two tandem cylinders near the wall using (PIV). The results showed that a low-velocity region creates behind the cylinders as gap height decreased to 0.3. A summary of the above and some previous experimental studies of flow around the cylinder near the wall is summarized in Table 1. In this table, it can be seen that some researchers have investigated the effect of gap height on vortex shedding, drag, lift or pressure fluctuations in different Reynolds numbers for circular and square cylinders. However, there are few experimental studies about flow structure to explain how this method leads to heat transfer enhancement. In addition, in Table 1, it is observed that PIV has become a popular method for determination of flow structure around the bluff bodies in recent years. This method is able to show more details about the flow near a wall past the inserts.

The present study aims to use PIV measurement and POD analysis to present flow structure near the flat plate behind a square cylinder. PIV measurement and POD analysis were employed for the explanation of the heat transfer enhancement. In addition, for the comprehensive understanding of heat transfer characteristics of the phenomena, the temperature sensitive paint (TSP) method is applied for the determination of the temperature distribution of the flat plate. The TSP is a polymer-based paint in which the temperature-sensitive luminescent molecules are immobilized. The quantum efficiency of luminescence decreases with increasing temperature; this effect associated with temperature is thermal quenching that serves as the major working mechanism for the TSP.

TABLE 1. A summary of experimental studies of flow around the cylinder near the wall using different techniques

Measured variable	Cylinder type	Measurement technique	Re	G/D	References
Strouhal number	Circular	HWA	2.5-4.5×10^4	0-3.5	[15]
Strouhal number	Circular	HFA- PIV	1200–4960	0-2	[19]
Darg and Lift	Square	LDA HWA	18900	0.1-1.6	[16]
Strouhal number	Circular-Square	PIV	1.4×10^4	0.1-1	[20]
Wall-pressure fluctuations	Square	HFA	13200	0.25 & 0.5	[21]
Velocity measurement	Square	S-PIV, TR-PIV	2250	0.1-0.8	[17]
Wall-pressure fluctuations	Square	Microphone	13,200	0.25 & 0.5	[22]
Vorticity	Circular	PIV	8700	0.15-1	[23]
Velocity field	Circular	PIV	3036-3924	0.8	[24]
Velocity field	Circular	PIV	4.9×10^3	0.3-3	[18]
Velocity field	Circular	PIV	6×10^4	0.05-1.5	[25]

2. EXPERIMENTAL DATAILS

The recently developed low-velocity open-circle wind tunnel was used for testing [22]. The settling compartment contained sequentially a honeycomb and five screens. The flow was straightened via contraction ratio of 6:1 from a diffuser and a smooth contraction fairing. The inlet channel was 300 mm (width) × 300 mm (height) × 1000 mm (length) in dimensions. A 1.5 kW motor and a centrifugal blower drove air. The dimensions of the test section were 300 (width)× 300 mm (height) ×1240 mm (length). An inverter (Danfoss, Denmark) was applied to manage the flow rate in the test section.

The 2D square cylinder (10 mm × 10 mm), spanning the entire the test section width, in 220-mm downstream station of the leading edge is presented in Figure 1. The cylinder diameter (D)-based Reynolds number (Re_D) of 5130 was achieved by the constant free-stream velocity of 8 m/s. The intensity of free-stream turbulence was less than 0.6%. The δ/D of 1.5 was obtained for the thickness of the boundary layer (δ) at the cylinder location in lack of the cylinder. The optical access for PIV measurements can be provided by the plexiglas sidewalls of the wind tunnel channel. The planar PIV was used to measure the fluid flowing surrounding to the cylinders. An aerosol atomizer (PIV Part 14, PIVTEC-GmbH, Germany)-driven droplets of Di-Ethyl-Hexyl-Sebacat (DEHS) was applied for the global seeding of the complete wind tunnel volume. This phenomenon can result in a distribution of polydisperse with a mean diameter of about 1μm. A closed plexiglas tunnel covered completely the wind tunnel to provide the stable and homogeneous distribution of the seeding particles cross the long series of PIV measurements, which hereby closed-loop circulation is produced for the seeded air flow. About 10 times cross-sectional size was seen for the large tunnel compared to the test section. A high-quality pattern of seeding was achieved in the PIV images by adding DEHS droplets to the closed tunnel and then circulating the airflow for some minutes. An Nd:YAG laser at 135 mJ/pulse (532 nm, 8 ns, Litron, UK) illuminated the middle plane of the test section. A light sheet with 1 mm in thick was generated through the laser fitted with the compacted cylindrical lenses combination (Dantec, Danmark). The patterns of flow seeded in two adjacent areas were captured simultaneously by two synchronized CCD cameras, whose profiles were IPX 11M with 4000 × 2672 pixels (IMPERX, USA) and IPX 16M with 4872× 3248 pixels (IMPERX, USA). Figure 1 shows a field-of-view of 60D × 17D with an overlapped region of 6 D resulting from the two separate CCD cameras with the help of two six-freedom positioning platforms. The seeded images were integrated with an imaged pattern in a flash

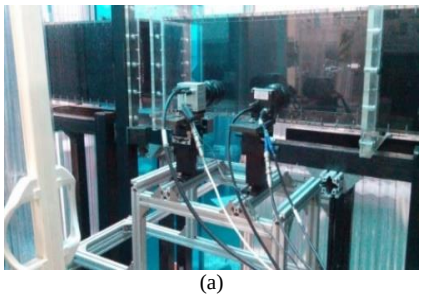

(a)

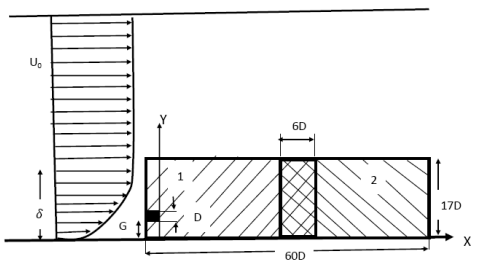

(b)

Figure 1. (a) Schematic diagram of the PIV setup, (b) PIV measurement regions

using post-processing imaging. A pulse delay generator was employed to synchronize of the double-pulsed laser with the two CCD cameras. The synchronization of CCD cameras and the laser occurs following the order of pico-seconds seen for the inherent inter-channel interval of the generator.

Totally, 3000 images were recorded using the cameras within the experiment. The size of 32 ×32 pixels was reported for the interrogation window while having 50% overlap, which leads to a measurement grid of velocity vectors with 1 mm ×1mm spacing. The signal/noise ratio was improved through the standardized cross-correlation algorithm combined with window-offset, Gaussian fitting-recognized by sub-pixel and sub-region distortion.

For temperature measurement, the TSP method was used. Schematic diagram of the TSP setup, measurement region and dimensions of the heater is shown in Figure 2. The heater module is produced using Kapton heater, and its maximum power was obtained 300 W. To obtain constant heat flux, a thin aluminum plate was connected on the top surface of Kapton heater by high thermal conductivity glue. The bottom of the heater was insulated by an elastic insulation with a thermal conductivity less than 0.04 W/m^2.k to avoid the heat loss through the bottom. The power supply of the heater was adjusted on 100 W. Ru(bby) was employed as a TSP luminophore with maximum emission around 600nm, and Dupont Chromeaclear HC-7776S was selected as a TSP binder. An LED unit was used as an exciting light with 400 nm wavelength and the luminescence from the sensor was detected by a CCD camera with 4000 × 2672 pixels and 200 ms exposure

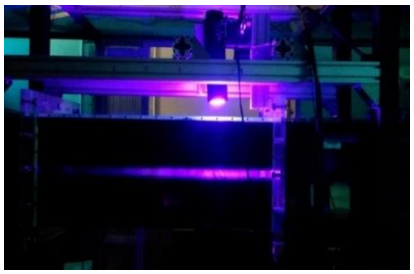

(a)

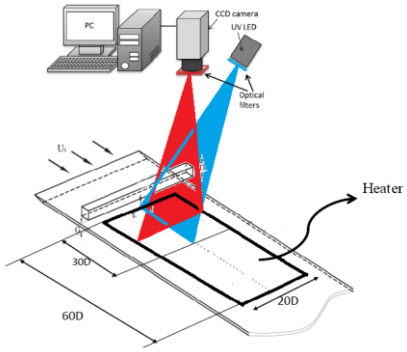

(b)

Figure 2. (a) Schematic diagram of the TSP setup, (b) TSP measurement region

time. At each measurement, 20 pictures were obtained and then averaged to decrease the shot noise. In two points of the surfacer, the temperature has been measured by two thermocouples for the calibration between the temperature and the luminescent intensity.

After obtaining the surface temperature distribution, the local heat transfer coefficient can be calculated based on the following equations:

$$q = VI \tag{1}$$

$$h = \frac{q}{(T_S - T_\infty)} \tag{2}$$

3. RESULTS AND DISCUSION

To validate the current results, the comparison of the normalized heat transfer coefficients for the current study and reported data [5] is shown in Figure 3. It can be seen that the current study has a good agreement with the reported data [5].

In Figure 4, the temperature distribution is shown for five cases i.e., without cylinder, G/D=0.8, G/D=0.2, G/D=0.1, and G/D=0.0. For the case without the cylinder, as the thickness of the boundary layer is almost constant in the turbulent boundary layer, temperature variations are taken into account very slightly. For the cases with the cylinder, it is observed that surface temperature decreases in most of the regions. For the case G/D=0.8, in the region (0<X/D<8), temperature values are smaller than values for the case without cylinder. While, in the region (8<X/D<15), temperature values for the two cases are close to each other.

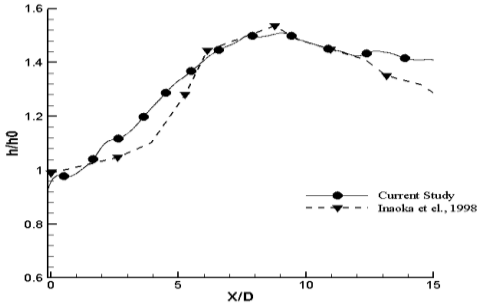

Figure 3. Comparison of the normalized heat transfer coefficients for current study and result of [5]

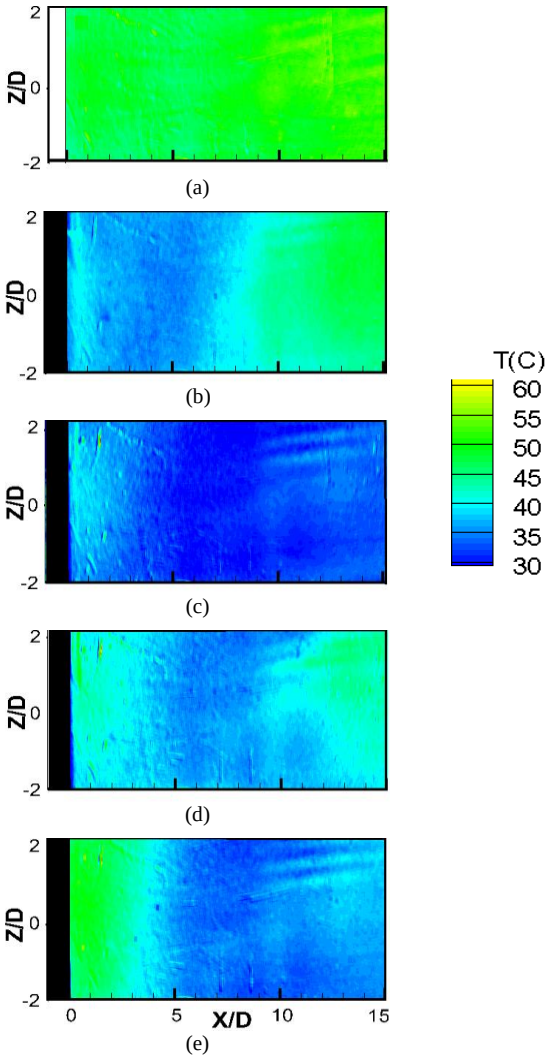

(a) (b) (c) (d) (e)

Figure 4. Temperature distribution of heated surface behind the square cylinder: (a) Without cylinder, (b) G/D = 0.8, (c) G/D = 0.2, (d) G/D = 0.1 and (e) G/D = 0.0

For the case G/D=0.2, temperature values are noticeably smaller than values for the other cases in all points. For the case G/D=0.1, in most of the regions, the surface temperature is smaller than that for the cases without cylinder and G/D=0.8. For the case G/D=0.0, in the region (X/D<3), the surface temperature is larger than that for the other cases with the cylinder. While, in the region (X/D>3), temperature values for this case are significantly smaller than values for the case G/D=0.8.

Figure 5 shows the local heat transfer coefficient, h, normalized by the heat transfer coefficient of the case without the cylinder, h_0. It is observed that the insertion of a square cylinder leads to increase the heat transfer in most of the regions for all the cases. For the case G/D=0.8, heat transfer is weakly enhanced in the region (0<X/D<8). Also, in the region (8<X/D<15), the square cylinder has not affected the heat transfer enhancement. For the case G/D=0.2, values of the heat transfer enhancement are significantly larger, as compared to those for the other cases, for all X/Ds. Also, at (X/D=8), heat transfer coefficient becomes twice the value of h_0. For the case G/D=0.1, h has a value less than h_0. Also, for the case G/D=0.0, in the region (0<X/D<3), reduction of the heat transfer is taken into account. However, for these cases (G/D=0.1 and G/D=0.0), at (X/D=8), values of the heat transfer enhancement become more than 50% and 60%, respectively.

Time-averaged streamlines of the flow past the square cylinder are demonstrated in Figure 6. For the case G/D=0.8, two time-mean recirculation regions with a small asymmetry is observed after the cylinder. As these recirculation zones are far from the surface, they cannot exert a major influence on the surface heat transfer coefficient. By decreasing the gap height to G/D=0.2, the symmetry of two recirculation zones decreases and a separation flow is created in the region (2<X/D<6) near the wall. When the separated flow is unsteady, it mixes fluids inside and outside the separated flow and improves the heat transfer coefficient. In addition, a flow reattachment occurs at (X/D=6), which has a washing action effect on the surface. Because, as shown in Figure 4(c), the surface temperature is seen to decrease near the (X/D=6).

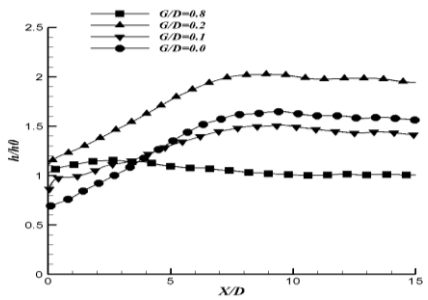

Figure 5. Comparison of normalized heat transfer coefficients behind the square cylinder

By decreasing the gap height to G/D=0.1, the wake pattern considerably changes due to the elimination of the vortex shedding. A single recirculation zone is located instantly behind the cylinder, with its width and length equal to the square cylinder size. Moreover, a strong separated flow forms near the wall in the region (2<X/D<6). As it mentioned above, unsteadiness manner of the separated flow can augment heat transfer coefficient. Based on Figure 4(d), heat transfer is enhanced in the region (2<X/D<6). In addition, like the case G/D=0.2, a reattachment point is observed at (X/D=6) that is the location of deterioration of the temperature value in Figure 4(d). For the last case, the square cylinder attached to the surface, the recirculation region behind the cylinder is removed, and only the separated flow instantly behind the cylinder expands to X/D=6. However, in the region (0<X/D<3), its heat transfer coefficient (Figure 5) is smaller than that in the case without cylinder. This could be attributed to the steady behavior of the separated flow. In this case, like the cases G/D=0.1 and G/D=0.2, the flow reattachment point occurs at (X/D=6), where, based on Figure 4(e), reduction of the surface temperature is observed.

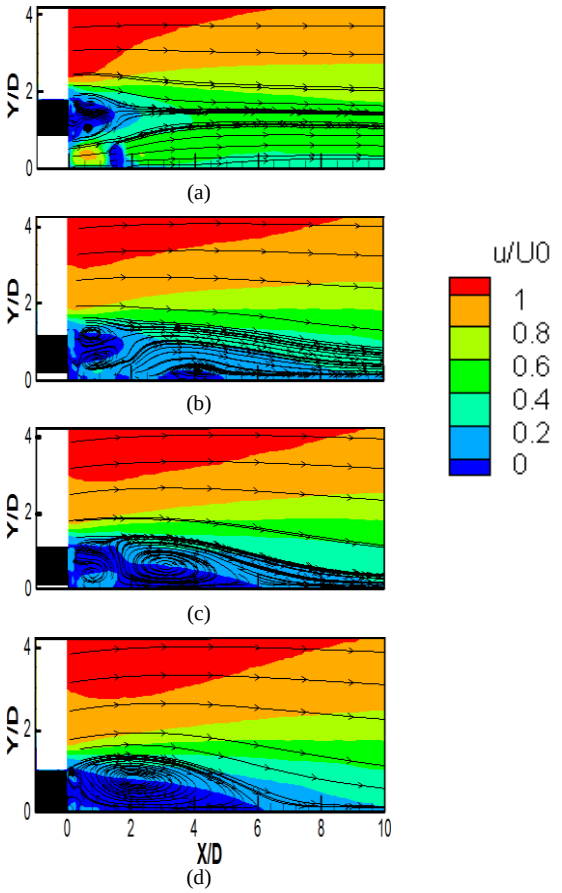

Figure 6. Time-mean streamline patterns of the wake behind the square cylinder: (a) G/D = 0.8, (b) G/D = 0.2, (c) G/D = 0.1 and (d) G/D = 0. 0

Therefore, for the three last cases (G/D=0.2, G/D=0.1, and G/D=0.0), the reattachment point plays a critical role in the heat transfer enhancement. As mentioned in Figure 6, in the three cases G/D=0.2, G/D=0.1, and G/D=0.0, near the wall, the separated flow behind the square cylinder is observed. However, based on Figure 4, only for the case G/D=0.2, heat transfer significantly increases where the separated flow occurred (2<X/D<6). This behavior can be due to the unsteady manner of the separated flow. To study the separated flow behavior, the reverse flow intermittency (γ_t) is shown in Figure 7.

A fraction of the realization in which the flow is reversed in a given position is called the intermittency [26]. It can be said that the most unstable nature of the flow is due to the 50% share in a time of forward and reversed flow regarding the reverse-flow intermittency of 0.5 [19]. Therefore, highly unstable flow in the following discussion can be associated with the central green band of 0.4<γ_t<0.6. For the case G/D=0.8, a reverse flow focused at the recirculation region behind the cylinder. The inverse swirling vortices released alternatively by upper and lower regions cause highly unstable fluid flow around the recirculation region. In addition, in the region close to the bottom plane wall (1<X/D<2), the unstable reverse flow (0.4<γ_t<0.6) is resulted from the effect of the wall on vortices shed from the lower side. For the case G/D=0.2, distribution at two recirculation zones is almost like that for the case G/D=0.8, but with more stability due to the effect of the wall neighborhood. However, the highly unstable reverse flow (0.4<γ_t<0.6) near the surface expands to X/D=6 that plays an important role in heat transfer between hot fluids near the wall and cold fluid far from the wall. Therefore, the surface temperature reduction, as shown in Figure 4(c), in the region (2<X/D<6) is due to this unstable reverse flow. For the case G/D=0.1, it is observed that the separated flow becomes more stable than that for the case G/D=0.2 in the region (2<X/D<5). Therefore, for the case G/D=0.1, as shown in Figure 4(d), in this region, the surface temperature is larger than that for the case G/D=0.2. For the case G/D=0.0, the separated flow becomes highly stable (γ_t>0.8) in the region (0<X/D<4). Therefore, fluid temperature becomes rather high in this region, which has a negative effect on heat transfer. As a result of this, heat transfer coefficient, as shown in Figure 5, in the region (0<X/D<3) is lower than that of the case without cylinder.

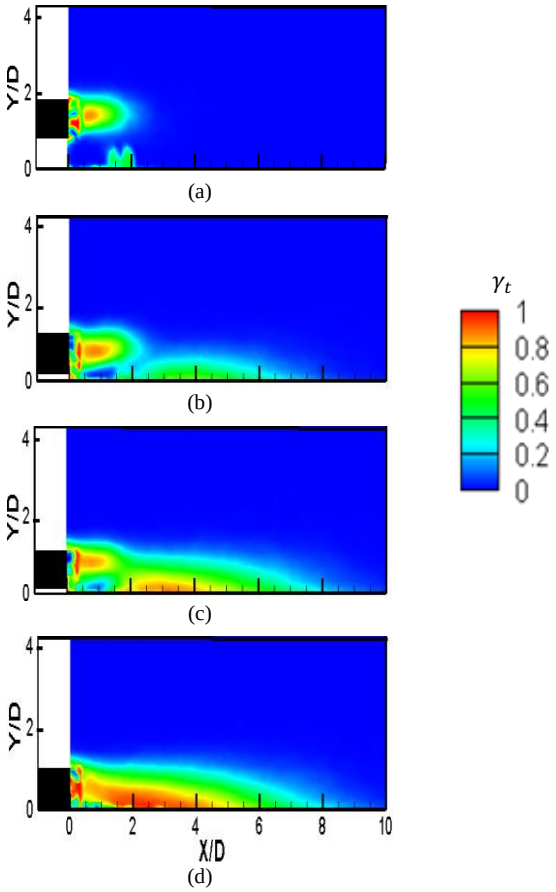

Figure 7. Distribution of reverse-flow intermittency of the wake behind the square cylinder: (a) G/D = 0.0, (b) G/D = 0.1, (c) G/D = 0.2 and (d) G/D = 0.8

In Figure 8, a Reynolds shear stress behind the square cylinder is depicted. As shown in the figure, two shear layers are created on the lower and upper sides of the cylinder. For all the cases, the upper shear layer (USL) is highly stronger than the lower shear layer (LSL) due to the effect of the wall on the LSL. For the case G/D=0.8, the intensity of the USL is 6 times stronger than that of the LSL. The LSL leads to heat transfer enhancement by increasing the rate of flow mixing near the wall. By comparison of Figures 4(b) and 8, for this case, it is concluded that the heat transfer enhancement in the region (0<X/D<3) is due to the intensity of the LSL. Therefore, for the case G/D=0.8, the LSL is an effective factor in the heat transfer enhancement. By decreasing the gap height, the shear layers are weakened due to the wall effects. Also, against the LSL, reduction of the Reynolds stress in the upper one is slower because of the free release of the vortices. By decreasing the gap height to G/D=0.2 and G/D=0.1, the thickness of the shear layers also greatly decreases. For the case G/D=0.0, the LSL is almost removed.

In Figure 9, contours of normal velocity fluctuations behind the square cylinder are displayed for four gap heights. For the case G/D=0.8, the intensity of velocity fluctuations in both the upper and lower sides of the cylinder is significant. The normal velocity fluctuation on the LSL is a direct factor for heat transfer between the plate and free stream. Therefore, once more, it is concluded that the LSL is a significant factor in heat

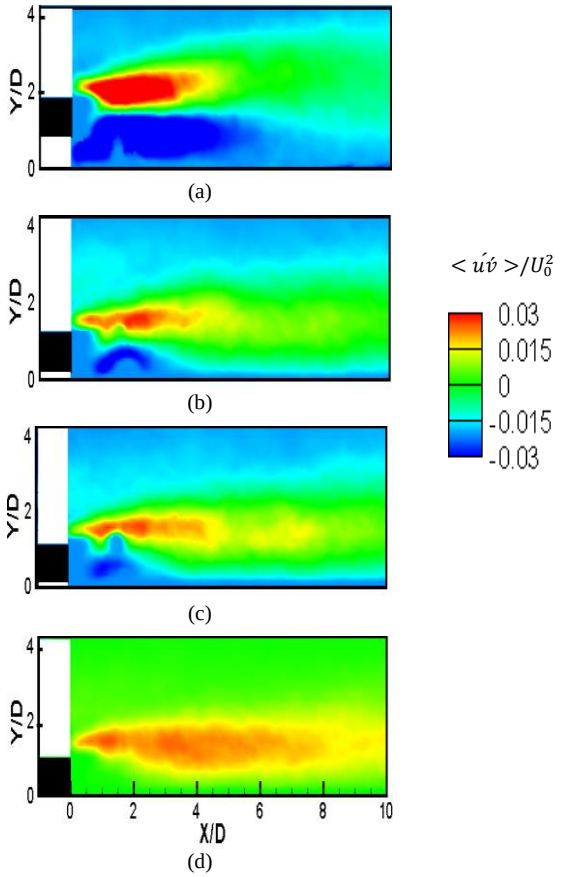

Figure 8. Contours of shear stress behind the square cylinder: (a) G/D = 0.8, (b) G/D = 0.2, (c) G/D = 0.1 and (d) G/D = 0.0

transfer enhancement for this case. By decreasing the height, for the case G/D=0.2, the thickness of the two shear layers is reduced due to the wall neighborhood. For the case G/D=0.1, the intensity of the normal velocity fluctuations becomes 50% of that for the case G/D=0.8. For the case G/D=0.0, the LSL is almost removed and therefore, the effect of the normal velocity fluctuation is considerably weakened by the wall effects.

The POD decomposed totally 3000 snapshots of the vector fields obtained from the standard PIV. The eigenvalue of the first 10 eigenmodes representing the comparative portion of the mode to the fluctuation energy of the flow field is shown in Figure 10. As can be seen, initially decrease occurs sharply in the eigenvalue by increasing mode number for the first some eigenmodes, followed by gradual reduction. In contrast, increasing mode number sharply leads to increase initially in the cumulative energy for the first some eigenmodes. However, the convergence rate decreases by increasing eigenmodes. The poor vortex shedding process close to the wall could probably result in the reduction in the dominance of the first two modes by decreasing the gap from G/D of 0.8 to 0.2. Nevertheless, the reduced gap from G/D of 0.2 to 0.1 resulted in the high dominance of the first two modes might be justified by increasing and shedding large-scale vertical structures weakened in the USL coping with the other unsteady behaviors similar to the flapping motion of the separated shear layer [17]. No significant difference can be found for eigenvalues with G/D of 0.0 compared to those with G/D of 0.2, probably because of the same impact of wall neighborhood on the vortex shedding for both items.

Based on the four cases in Figure 10, it is concluded that the first two eigenmodes coincide with specified of the largest-scale characteristics of the flow pattern. In Figure 11, the vector patterns of the first two eigenmodes are shown for all gap heights. It is observed that the common Karman-vortex shedding treatment is still dominant at G/D= 0.8, while more asymmetry is observed at G/D= 0.2. For the other two cases G/D = 0.1 and 0.0, the low-order flow patterns are very similar and no obvious treatment of vortex shedding proceeding can be represented. Also, by comparison of the four cases, only for G/D=0.2, the reverse flow occurs for both the two modes near the wall behind the square. This behavior confirms that reverse flow near the wall behind the square is highly unstable for this case.

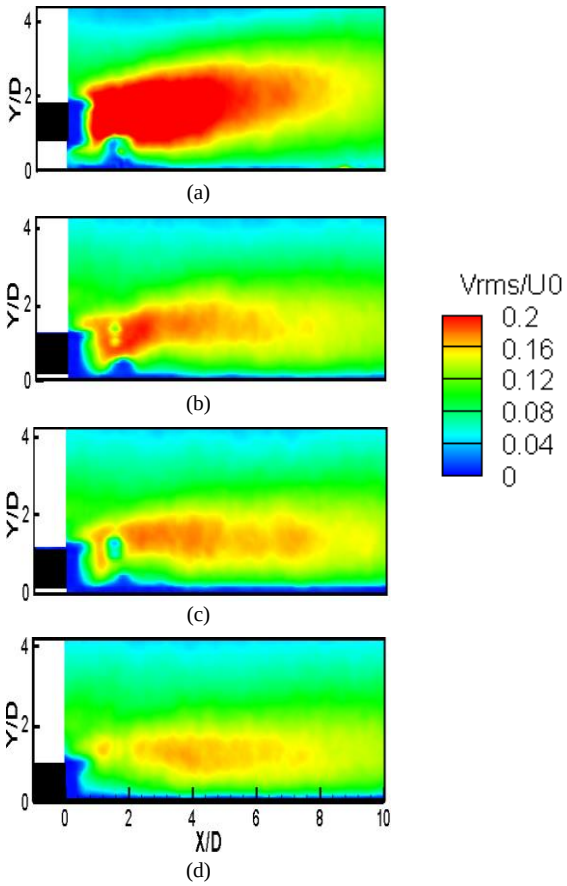

Figure 9. Contours of normal velocity fluctuations behind the square cylinder: (a) G/D = 0.8, (b) G/D = 0.2, (c) G/D = 0.1 and (d) G/D = 0.0

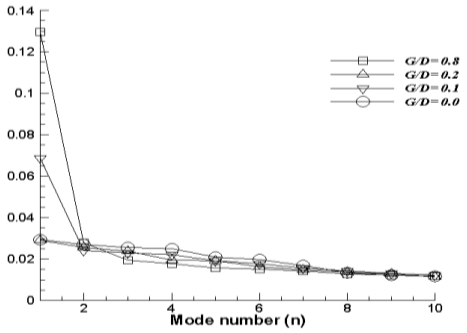

Figure 10. Normalized eigenvalues of the first 10 eigenmodes

4. CONCLUSION

In this study, the flow structure behind the square cylinder near the flat plate was investigated using PIV measurement and POD analysis for four gap heights. Also, the temperature distribution of the flat plate is obtained by the TSP method. These measurements were performed to present reasons for the heat transfer enhancement behind the square cylinder. The following conclusions were obtained from the analysis of the results:

1. For the case G/D=0.2, temperature values are noticeably smaller than values for the other cases in all points.
2. For the case G/D=0.2, at (X/D=8), heat transfer coefficient becomes twice the value of h_0.
3. For the three cases (G/D=0.2, G/D=0.1, and G/D=0.0), the reattachment point plays a critical role in the heat transfer enhancement.
4. Surface temperature reduction for the case G/D=0.2 in the region (2<X/D<6) is due to the unstable reverse flow.
5. For the case G/D=0.0, the stability of reverse flow in the region (0<X/D<4) has a negative effect on heat transfer.
6. For the case G/D=0.8, the LSL is a significant factor on heat transfer enhancement.
7. For the case G/D=0.2, the reverse flow occurs for both the two modes near the wall behind the square, confirming that the reverse flow near the wall behind the square is highly unstable.

5. ACKNOWLEDGMENT

This work was supported by Shanghai Jiao Tong University. I would like to thank our colleagues, especially Professor Ying Zheng Liu and Mr. Shao Fei Wang from Shanghai Jiao Tong University, who greatly assisted me in conducting this research by providing insight and expertise.

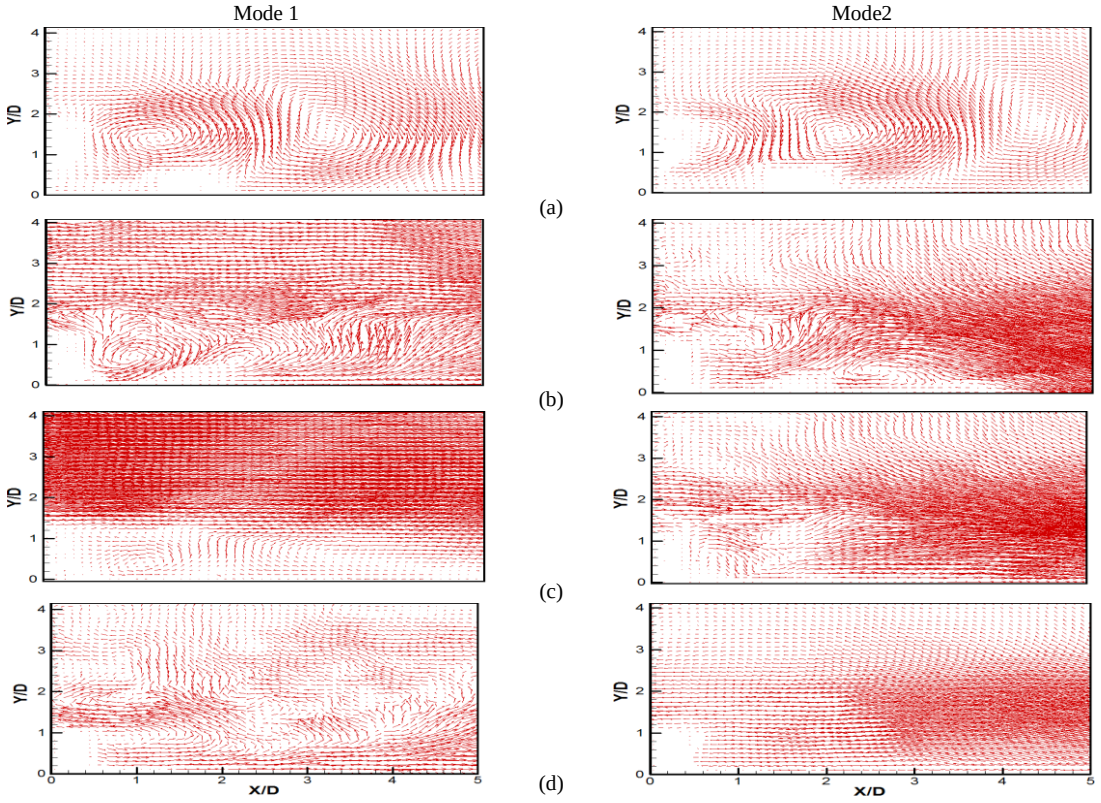

Figure 11. First two POD eigenmodes, (a)G/D=0.8, (b) G/D=0.2, (c)G/D=0.1, (d) G/D=0.0

6. REFERENCES

1. Marumo, E., Suzuki, K., and Sato, T., "Turbulent heat transfer in a flat plate boundary layer disturbed by a cylinder", ***International Journal of Heat and Fluid Flow***, Vol. 06, No. 4, (1985), 241–248.
2. Suzuki, H., Suzuki, K., and Sato, T., "Dissimilarity between heat and momentum transfer in a turbulent boundary layer disturbed by a cylinder", ***International Journal of Heat and Mass Transfer***, Vol. 31, No. 2, (1988), 259–265.
3. Suzuki, H., Suzuki, K., Kikkawa, Y., and Kigawa, H., "Heat transfer and skin friction of a flat plate turbulent boundary layer disturbed by a cylinder", ***Heat transfer. Japanese research***, Vol. 20, No. 2, (1991), 97–112.
4. Inaoka, K., Yamamoto, J., and Suzuki, K., "Dissimilarity between heat transfer and momentum transfer in a disturbed turbulent boundary layer with insertion of a rod - modeling and numerical simulation", ***International Journal of Heat and Fluid Flow***, Vol. 20, No. 3, (1999), 290–301.
5. Inaoka, K., Yamamoto, J., and Suzuki, K., "Heat Transfer Characteristics Of A Flat Plate Laminar Boundary Layer Disturbed By A Square Rod", In International conference on advanced computational methods in heat transfer, Poland, (1998), 297-306.
6. Inaoka, K., Mesaru, M., and Suzuki, K., "Flow and Heat Transfer Characteristics of a Turbulent Boundary Layer with an Insertion of a Square Rod (Control of Vortex Shedding by a Splitter Plate)", ***Transactions of the Japan Society of Mechanical Engineers***, Vol. 97, No. 4, (1998), 212–218.
7. Kahrom, M., Farievar, S., and Haidarie, A., "The Effect of Square Splittered and Unsplittered Rods in Flat Plate Heat Transfer Enhancement", ***International Journal of Engineering - Transactions A: Basics***, Vol. 20, No. 1, (2007), 83–94.
8. Razavi, S.E., Shafaghi, A.H., and Piroozfam, N., "Numerical Study on Hydrodynamics and Heat Transfer Characteristics Around a Cylinder with Inclined Splitter Plates", ***International Journal of Engineering - Transactions A: Basics***, Vol. 29, No. 4, (2016), 546–553.
9. De Souza, F., Delville, J., Lewalle, J., and Bonnet, J., "Large scale coherent structures in a turbulent boundary layer interacting with a cylinder wake", ***Experimental thermal and fluid science***, Vol. 19, No. 4, (1991), 204–213.
10. Kahrom, M., Haghparast, P., and Javadi, S., "Optimization of Heat Transfer Enhancement of a Flat Plate Based on Pareto Genetic Algorithm", ***International Journal of Engineering - Transactions A: Basics***, Vol. 23, No. 2, (2010), 177–190.
11. Kahrom, M., and Javadi, S., "Application of Single Objective Genetic Algorithm to Optimize Heat Transfer Enhancement from a Flat Plate", ***International Journal of Engineering- Transactions C: Aspects***, Vol. 25, No. 1, (2012), 67–78.
12. Ghassabi, G., and Kahrom, M., "Optimization of Heat Transfer Enhancement of a Domestic Gas Burner Based on Pareto Genetic Algorithm: Experimental and Numerical Approach", ***International Journal of Engineering - Transactions A: Basics***, Vol. 26, No. 1, (2012), 59–72.
13. Ghorbani-Tari, Z., Chen, Y., and Liu, Y., "End-wall heat transfer of a rectangular bluff body at different heights: Temperature-sensitive paint measurement and computational fluid dynamics", ***Applied Thermal Engineering***, Vol. 122, (2017), 697–705.
14. Ghorbani-Tari, Z., Yujia, C.H.E.., and Yingzheng, L.I.., "Complementary temperature-sensitive paint measurements and CFD analysis of wall heat transfer of cubes-in-tandem in a turbulent channel flow", ***Experimental Thermal and Fluid Science***, Vol. 98, (2018), 56–67.
15. Bearman, P.W., and Zdravkovich, M.M., "Flow around a circular cylinder near a plane boundary", ***Journal of Fluid Mechanics***, Vol. 89, No. 1, (1978), 33–47.
16. Martinuzzi, R.J., Bailey, S.C.C., and Kopp, G.A., "Influence of wall proximity on vortex shedding from a square cylinder", ***Experiments in Fluids***, Vol. 34, No. 5, (2003), 585–596.
17. Shi, L.L., Liu, Y.Z., and Wan, J.J., "Influence of wall proximity on characteristics of wake behind a square cylinder: PIV measurements and POD analysis", ***Experimental Thermal and Fluid Science***, Vol. 34, No. 1, (2010), 28–36.
18. Raiola, M., Ianiro, A., and Discetti, S., "Wake of tandem cylinders near a wall", ***Experimental Thermal and Fluid Science***, Vol. 78, (2016), 354–369.
19. Price, S.J., Sumner, D., Smith, J.G., Leong, K., and Paidoussis, M.P., "Flow visualization around a circular cylinder near to a plane wall", ***Journal of Fluids and Structures***, Vol. 16, No. 2, (2002), 175–191.
20. Wang, X.K., and Tan, S.K., "Comparison of flow patterns in the near wake of a circular cylinder and a square cylinder placed near a plane wall", ***Ocean Engineering***, Vol. 35, No. 5–6, (2008), 458–472.
21. Shi, L.L., Liu, Y.Z., and Sung, H.J., "On the wake with and without vortex shedding suppression behind a two-dimensional square cylinder in proximity to a plane wall", ***Journal of Wind Engineering and Industrial Aerodynamics***, Vol. 98, No. 10–11, (2010), 492–503.
22. Liu, Y.Z., Shi, L.L., and Zhang, Q.S., "Proper orthogonal decomposition of wall-pressure fluctuations under the constrained wake of a square cylinder", ***Experimental Thermal and Fluid Science***, Vol. 35, No. 7, (2011), 1325–1333.
23. Khabbouchi, I., Guellouz, M.S., and Ben Nasrallah, S., "A study of the effect of the jet-like flow on the near wake behind a circular cylinder close to a plane wall", ***Experimental Thermal and Fluid Science***, Vol. 44, (2013), 285–300.
24. Hsieh, S.C., Low, Y.M., and Chiew, Y.M., "Flow characteristics around a circular cylinder subjected to vortex-induced vibration near a plane boundary", ***Journal of Fluids and Structures***, Vol. 65, (2016), 257–277.
25. Zang, Z., and Zhou, T., "Transverse vortex-induced vibrations of a near-wall cylinder under oblique flows", ***Journal of Fluids and Structures***, Vol. 68, (2017), 370–389.
26. Cao, S., and Tamura, T., "Experimental study on roughness effects on turbulent boundary layer flow over a two-dimensional steep hill", ***Journal of Wind Engineering and Industrial Aerodynamics***, Vol. 94, No. 1, (2006), 1–19.

Heat Transfer Enhancement of a Flat Plate Boundary Layer Distributed by a Square Cylinder: Particle Image Velocimetry and Temperature-Sensitive Paint Measurements and Proper Orthogonal Decomposition Analysis

G. Ghassabi[a], M. Kahrom[b]

[a] *Department of Mechanical Engineering, Engineering faculty, Bozorgmehr University of Qaenat, Qaen, Iran*
[b] *Department of Mechanical Engineering, Ferdowsi University of Mashhad, Mashhad, Iran*

P A P E R I N F O

Paper history:
Received 06 July 2018
Received in revised form 22 August 2018
Accepted 26 October 2018

Keywords:
Heat transfer coefficient
Reverse flow
Reattachment point
Eigenmode

چکیده

مطالعه تجربی حاضر، بررسی تاثیردیواره بر ساختار جریان و افزایش انتقال حرارت پشت یک مربع می‌باشد. یک تونل مدار باز کم سرعت برای آزمایش در عدد رینولدز ۵۱۳۰ بر مبنای قطر سیلندر، استفاده شده است. چند فاصله بین مانع و دیواره مختلف (G/D=0.0, 0.1, 0.2, 0.8) برای مقایسه نتایج درنظر گرفته شده است. اندازه‌گیری میدان جریان با استفاده از روش سرعت‌سنجی تصویری ذرات (PIV) بوسیله دوربین با تعداد عکس زیاد صورت گرفته است. خروجی‌های میانگین زمانی بدست آمده از روش *PIV* شامل خطوط جریان، شدت نوسانات سرعت و تابع تناوب جریان معکوس برای جریان پشت مانع مورد بررسی قرار گرفتند اندازه‌گیری‌های PIV به کمک روش تجزیه متعامد متناسب (POD) دیدگاه مناسب از مدهای انرژی POD فراهم می‌کند. برای تعیین میزان افزایش انتقال حرارت پشت مانع، توزیع دمای صفحه تخت با استفاده از روش رنگ حساس به دما (TSP) محاسبه شده است. نتایج نشان می‌دهد ماکزیمم انتقال حرارت، برای حالت G/D=0.2 بدست آمده است که در نتیجه جریان برگشتی به شدت ناپایا می‌باشد.

***doi**: 10.5829/ije.2018.31.11b.21*